

Supporting Information for

Zn₃P₂S₈: A Promising Infrared Nonlinear-Optical Material with Excellent Overall Properties

Zhuang Li,^{a,b} Xingxing Jiang,^a Molin Zhou,^{a,b} Yangwu Guo,^{a,b} Xiaoyu Luo,^{a,b} Yicheng Wu,^{a,c} Zheshuai Lin,^a Jiyong Yao^{a,*}

^a Beijing Center for Crystal Research and Development, Key Laboratory of Functional Crystals and Laser Technology, Technical Institute of Physics and Chemistry, Chinese Academy of Sciences, Beijing 100190, P. R. China

^b University of Chinese Academy of Sciences, Beijing 100049, P. R. China

^c Institute of Functional Crystal Materials, Tianjin University of Technology Tianjin 300384, P.R. China

Corresponding author: Jiyong Yao; jyao@mail.ipc.ac.cn.

1. Syntheses of Zn₃P₂S₈

2. Property characterization

3. Figure S1. Crystal structure of LiZnPS₄; the blue, turquoise and yellow tetrahedra represent the (ZnS₄)⁴⁻, (PS₄)³⁻ and (LiS₄)⁷⁻ units, respectively

4. Figure S2. SEM (scanning electron microscope) image of Zn₃P₂S₈ crystal and element distribution.

5. Computational methods

6. References

Experimental details

1. Synthesis

ZnS (99.9%) and P₂S₅ (99.99%) were directly purchased from Sinopharm Chemical Reagent Co., Ltd. All manipulations were performed in an Ar-filled glovebox with H₂O and O₂ contents less

than 0.1 ppm. Polycrystalline sample of $\text{Zn}_3\text{P}_2\text{S}_8$ was obtained by traditional solid state reaction in a stoichiometric mixture of ZnS and P_2S_5 . The raw materials were loaded into fused-silica tubes and then, the ampoules were flame-sealed under a high vacuum of 10^{-3} Pa. The tubes were then placed in a computer-controlled furnace and heated to 673 K within 15 h, left for 48 h and, finally, the furnace was turned off.

2. Property Characterization

Powder X-ray Diffraction

The powder X-ray diffraction pattern of the as-obtained polycrystalline powder was performed at room temperature on a Bruker D8 Focus diffractometer with Cu K_α ($\lambda = 1.5418 \text{ \AA}$) radiation. The scanning step width of 0.1° and a fixed counting time 0.2 s/step were applied to record the patterns in the 2θ range of $10 - 70^\circ$.

Diffuse reflectance spectroscopy

A Cary 5000 UV-vis-NIR spectrophotometer with a diffuse reflectance accessory was used to measure the spectrum of $\text{Zn}_3\text{P}_2\text{S}_8$ and BaSO_4 (as a reference) in the range 300 nm (4.1 eV) to 1500 nm (0.83 eV).

Thermal Analysis

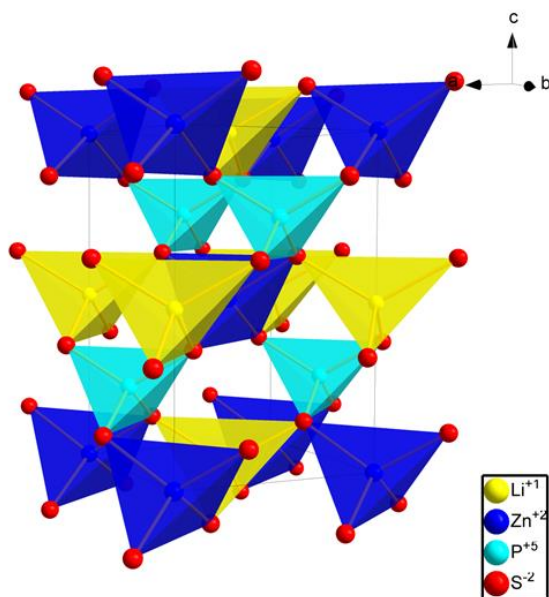
By applying the LabsysTM TG-DTA16 (SETARAM) thermal analyzer equipped with the nitrogen flow at a rate of about 30 ml/min, the thermal stability of $\text{Zn}_3\text{P}_2\text{S}_8$ was investigated in detail. Appropriate amounts of the polycrystalline powder were thoroughly ground, then were placed in a silica tube (5 mm o.d. \times 3 mm i.d.) and subsequently sealed under a high vacuum. The tube was heated from room temperature to 973 K and then cooled to room temperature with the heating/cooling rate both at 15 K min^{-1} .

SHG Measurement

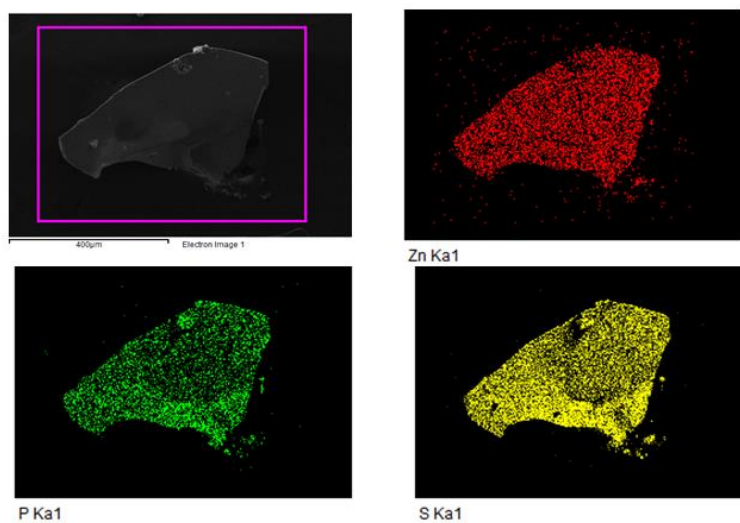
The optical SHG response of $\text{Zn}_3\text{P}_2\text{S}_8$ was measured by means of the Kurtz–Perry method.¹ The fundamental light was the 2090 nm light generated with a Q-switched Ho: Tm: Cr: YAG laser. The polycrystalline powder of $\text{Zn}_3\text{P}_2\text{S}_8$ was thoroughly ground and sieved into a series of distinct particle size ranges of 20 – 41, 41 – 74, 74 – 105, 105 – 150 and 150 – 200 μm , respectively,

which were then pressed into a disk with diameter of 8 mm that was put between glass microscope slides and secured with tape in a 1 mm thick aluminum holder. Microcrystalline AgGaS_2 was ground and sieved into the same particle size range of 150 – 200 μm as a reference.

3. **Figure S1.** Crystal structure of LiZnPS_4 ; the blue, turquoise and yellow tetrahedra represent the $(\text{ZnS}_4)^{4-}$, $(\text{PS}_4)^{3-}$ and $(\text{LiS}_4)^{7-}$ units, respectively



4. **Figure S2.** SEM (scanning electron microscope) image of $\text{Zn}_3\text{P}_2\text{S}_8$ crystal and element distribution.



5. Computational methods

The first-principles calculations are performed by the plane-wave pseudopotential method² based on density functional theory (DFT)³ implemented in the CASTEP package⁴. The ion-electron interactions are modeled by the optimized norm-conserving pseudopotentials⁵ for all constituent elements. A kinetic energy cutoff of 800 eV is chosen with Monkhorst-Pack k -point⁶ meshes spanning less than 0.04 per Å³ in the Brillouin zone. Based on the electronic band structure, the imaginary part of the dielectric function is calculated and the real part of the dielectric function is determined using the Kramers–Kronig transform, from which the refractive indices n (and the birefringence Δn) are obtained. Furthermore, The second order susceptibility $\chi^{(2)}$ and the second-harmonic generation (SHG) coefficients d_{ij} are calculated using an expression originally proposed by Rashkeev et al.⁷ and developed by Lin et al.⁸. The second-order susceptibility χ_{ijk} is represented as:

$$\chi_{ijk} = \chi_{ijk}^{(\text{VE})} + \chi_{ijk}^{(\text{VH})} + \chi_{ijk}^{(\text{twobands})}$$

where $\chi_{ijk}^{(\text{VE})}$ and $\chi_{ijk}^{(\text{VH})}$ denote the contributions from virtual-electron processes and virtual-hole processes, respectively, and $\chi_{ijk}^{(\text{two bands})}$ gives the contribution from two band processes to $\chi^{(2)}$. The formulas for calculating $\chi_{ijk}^{(\text{VE})}$, $\chi_{ijk}^{(\text{VH})}$ and $\chi_{ijk}^{(\text{two bands})}$ are as following:

$$\begin{aligned}\chi_{ijk}^{(\text{VE})} &= \frac{e^3}{2\hbar^2 m^3} \sum_{vcc'} \int \frac{d^3 \vec{k}}{4\pi^3} P(ijk) \text{Im}[p_{vc}^i p_{cc'}^j p_{c'v}^k] \left(\frac{1}{\omega_{cv}^3 \omega_{ve}^2} + \frac{2}{\omega_{ve}^4 \omega_{c'v}} \right) \\ \chi_{ijk}^{(\text{VH})} &= \frac{e^3}{2\hbar^2 m^3} \sum_{vv'c} \int \frac{d^3 \vec{k}}{4\pi^3} P(ijk) \text{Im}[p_{vv'}^i p_{v'c}^j p_{cv}^k] \left(\frac{1}{\omega_{cv}^3 \omega_{v'c}^2} + \frac{2}{\omega_{vc}^4 \omega_{cv'}} \right) \\ \chi_{ijk}^{(\text{twobands})} &= \frac{e^3}{\hbar^2 m^3} \sum_v \int \frac{d^3 \vec{k}}{4\pi^3} P(ijk) \frac{\text{Im}[p_{vc}^i p_{cv}^j (p_{vv}^k - p_{cc}^k)]}{\omega_{vc}^5}\end{aligned}$$

Here, i, j and k are Cartesian components, v and v' denote VB, and c and c' denote CB. $P(ijk)$ denotes full permutation. It should be emphasized that the refractive indices and SHG coefficients can be accurately obtained by DFT in principle because these optical properties are determined by the virtual electronic excited processes which are described by the first- and second-order perturbations, respectively, on the ground state wavefunctions.

References

- (1) Kurtz, S. K.; Perry, T. T. *J. Appl. Phys.* **1968**, *39*, 3798.
- (2) Payne, M. C.; Teter, M. P.; Allan, D. C.; Arias, T. A.; Joannopoulos, J. D. *Rev. Mod. Phys.* **1992**, *64*, 1045-1097.
- (3) Kohn, W. *Rev. Mod. Phys.* **1999**, *71*, 1253-1266.
- (4) Clark, S. J.; Segall, M. D.; Pickard, C. J.; Hasnip, P. J.; Probert, M. J.; Refson, K.; Payne, M. C. *Z. Kristallogr.* **2005**, *220*, 567-570.
- (5) Rappe, A. M.; Rabe, K. M.; Kaxiras, E.; Joannopoulos, J. D. *Phys. Rev. B* **1990**, *41*, 1227-1230.
- (6) Monkhorst, H. J.; Pack, J. D. *Phys. Rev. B* **1976**, *13*, 5188-5192.
- (7) Rashkeev, S. N.; Lambrecht, W. R. L.; Segall, B. *Phys. Rev. B* **1998**, *57*, 3905-3919.
- (8) Lin, J.; Lee, M. H.; Liu, Z. P.; Chen, C. T.; Pickard, C. J. *Phys. Rev. B* **1999**, *60*, 13380-13389.